New Materials, Compounds and Applications
Vol.9, No.2, 2025, pp.282-297
https://doi.org/10.62476/nmca.92282

AN ANALYSIS OF THERMOPLASTIC COMPOSITE RODS BY SEGMENTATION OF SEM IMAGES USING IMPROVED U-NET MODEL

Kamran Samet[1,2*], Nooshin Nemati[3]

[1]Department of Manufacturing Engineering, Faculty of Technology, Gazi University, Ankara, Turkiye
[2]Department of Subsystem Structural Analysis, Turkish Aerospace, Ankara, Turkiye
[3]Department of Computer Engineering, Faculty of Engineering, Ankara University, Ankara, Turkiye

Abstract. The segmentation of thermoplastic composite rods in SEM images is crucial for analysing and understanding their microstructures and optimizing their mechanical properties. This study proposes an improved U-Net deep learning model for accurate segmentation of SEM images of thermoplastic composite rods. The proposed model incorporates attention mechanisms and residual blocks to enhance feature extraction and improve segmentation performance in complex microstructural regions. XAI techniques, specifically Grad-CAM, are also utilized to visualize the model's decision-making process. The model is trained and evaluated on a dataset of SEM images, achieving high segmentation accuracy and demonstrating superior performance compared to traditional methods. The results indicate that the improved U-Net model is effective in SEM images, offering a reliable tool for thermoplastic composite material analysis.

Keywords: *Thermoplastic composite materials, thermoplastic composite rod surface analysis, segmentation of SEM images, deep learning.*

[*]***Corresponding Author:*** *Kamran Samet, Department of Manufacturing Engineering, Faculty of Technology, Gazi University, Ankara, Turkiye; Department of Subsystem Structural Analysis, Turkish Aerospace, Ankara, Turkiye, Tel.: +905053592432, e-mail: kamran.samet@gmail.com*

Received: *19 March 2025;* ***Accepted:*** *8 May 2025;* ***Published:*** *5 August 2025.*

1. Introduction

Thermoplastic composites are high-performance materials with numerous advantages, including durability, lightweight and chemical resistance (Diniță *et al.*, 2023). These composites are composed of thermoplastic matrix materials reinforced with fibers, textiles or particles, which enhance their mechanical properties. One of their key characteristics is the ability to soften when heated and retain their shape when cooled, making them suitable for various manufacturing processes while also offering cost efficiency (Jin *et al*., 2022). Due to their exceptional properties, such as high strength and resistance to environmental factors, thermoplastic composites are widely utilized in industries including automotive, aerospace, construction and medical devices. However, understanding their microstructures and internal components is crucial for optimizing production processes and predicting product performance (Vaidya *et al.*, 2023).

The analysis of thermoplastic composite rods plays a critical role in assessing their structural integrity and performance. These rods undergo various mechanical and environmental tests, after which their surface characteristics are examined using microscopic imaging. In the realm of aerospace engineering, tube-shaped structural components, such as thermoplastic composite rods, are of paramount importance due to their critical role in enhancing the load-bearing capabilities of various systems. These rods are essential in applications like flight control mechanisms, rotor assemblies and other structural frameworks, where they contribute significantly to maintaining the integrity and stability of the overall structure. The unique combination of lightweight properties and high strength offered by thermoplastic composite rods directly influences aircraft performance, making them a focal point for material optimization and innovation. As such, understanding their microstructural characteristics through advanced analysis techniques, such as SEM image segmentation, is vital for improving their mechanical properties and ensuring their reliability in demanding aerospace environments (Tucci *et al*., 2023).

In examining the internal structures of thermoplastic composites, high-resolution microscopy techniques such as Scanning Electron Microscopy (SEM) are frequently employed. SEM is an ideal tool for analyzing surface structures and microstructures in great details. By scanning a sample with a beam of electrons, SEM produces highly detailed images of the surface, typically used to examine structures at the micrometer level. These images allow researchers to observe critical microstructural features of composite materials, such as fiber arrangements, matrix-filled voids and bonding areas (Butenegro *et al*., 2023). SEM images are instrumental in evaluating surface morphology, analyzing the arrangement of microstructures and detecting defects or abnormalities in production processes. However, segmenting SEM images is a challenging task due to the high resolution and complexity of composite structures. The presence of different phases within composite materials (e.g., fibers and matrices) creates subtle distinctions in SEM images, necessitating precise segmentation techniques for accurate analysis (Elderfield *et al*., 2024).

Accurate segmentation of SEM images obtained from thermoplastic composites allows for the isolation of specific structural components, providing deeper insights into the material's mechanical properties (Samet *et al*., 2024). Segmentation helps classify different regions of the image, facilitating further analysis. However, SEM images present segmentation challenges due to high resolution, texture variation, noise and the dense arrangement of microscopic structures. Deep learning leverages large datasets and multi-layered neural networks to automatically learn hierarchical features from images, outperforming traditional segmentation methods. In recent years, deep learning techniques, particularly U-Net convolutional neural networks (CNNs) (Wu *et al*., 2017), have emerged as powerful tools for SEM image segmentation. U-Net (Ronneberger *et al*., 2015), widely used in biomedical image segmentation, has proven effective in handling high-resolution images. Its encoder-decoder architecture and skip connections preserve spatial details at different resolution levels, enabling precise segmentation of fine structures in SEM images.

To address the limitations of manual inspection and enhance segmentation accuracy in SEM images of thermoplastic composites, this study proposes an improved U-Net model for anomaly detection. Modifications to the U-Net architecture include integrating attention mechanisms to enhance feature map refinement and incorporating residual blocks to improve gradient flow during training. These improvements aim to enhance segmentation accuracy, particularly in complex regions with overlapping or fine structures. Additionally, Explainable Artificial Intelligence (XAI) techniques, specifically Grad-CAM, were employed to interpret model predictions. Grad-CAM generates class activation maps to highlight regions that contributed most to the model's segmentation decisions, ensuring transparency and aiding in performance validation.

Furthermore, a novel dataset comprising SEM images of thermoplastic composite rod surfaces has been created to train and evaluate the proposed model. The performance of the model is assessed through extensive experiments and the obtained results are compared with existing studies in the literature. The proposed modified U-Net architecture offers a powerful solution for improving segmentation accuracy in SEM images, which feature high resolution and complex microstructures. The contributions of the paper:

- A new dataset consisting of images of thermoplastic composite rods was created.
- An improved deep learning model was proposed for the segmentation and analysis of rod surfaces.

This paper is structured as follows: Section 2 presents a literature review, summarizing previous studies on the microstructural analysis of thermoplastic composites and SEM image segmentation. Section 3 describes the proposed methodology in detail, including architectural improvements to the U-Net model. Section 4 is about results and discusses the segmentation performance of the proposed model and compares it with existing methods in the literature. Finally, Section 5 provides conclusions, highlighting the contributions of this study and suggesting directions for future research.

2. Related Works

Some studies have explored the segmentation of SEM images of thermoplastic composites and the identification of their structural components using deep learning models. A summary of some existing works is presented as follows:

Segmenting porous structures in FIB/SEM tomography is challenging due to shine-through artifacts, which hinder accurate material boundary detection. To address this issue, Moroni and Thiele (2020) have proposed an optical flow-based segmentation method that utilizes these artifacts. The effectiveness of this approach was demonstrated using tomographic datasets from a polymer electrolyte fuel cell catalyst layer and a lithium-ion battery composite electrode. Compared to manual segmentation, the method has achieved an accuracy of 0.866 and a precision of 0.84 for the catalyst layer. Dubey et al. (2024) investigated the impact of infill patterns 78 on the mechanical and viscoelastic properties of short carbon fiber-reinforced nylon composites (SCFRNCs) 79 produced via FDM. Tensile, flexural and DMA tests were conducted using grid, triangular, sinusoidal, hon-80 eycomb and rectilinear patterns. MicroCT analyzed internal structures, while SEM examined fracture sur-81 faces. With constant printing parameters, the rectilinear pattern achieved the highest tensile strength (34.58 82 MPa) and the triangular pattern showed the highest flexural strength (23.45 MPa). TGA indicated a 7.27% 83 fiber volume fraction. In DMA, the triangular pattern exhibited superior storage moduli: 747 MPa (tensile) 84 and 1280 MPa (flexural).

Mohsenzadeh et al. (2024) have proposed a computer vision-based method for particle size measurement to predict the elastic modulus of polymer nanocomposites. The method uses morphological segmentation to address limitations of idealized monodispersed particle assumptions. Particle sizes from SEM images of fractured surfaces have been applied in a finite element model for polyethylene/nano zeolite composites. Inter-phase thickness was estimated with the Hashin-Shtrikman model and modulus was calculated using a hybrid Hashin-Maxwell model. Finite element simulations showed a 0.329 deviation from experimental tensile modulus results, confirming the method’s accuracy. Lu et al. (2024) investigated pore segmentation in SEM images of the char layer from non-halogenated flame retardants, addressing limited sample sizes through data augmentation and transfer learning. Their findings indicate that CNN-based segmentation algorithms outperform traditional methods in accuracy, with offline data augmentation providing greater stability. Using transfer learning with VGG backbone weights, the model has achieved a pixel accuracy of 0.9449 and an intersection over union (IoU) of 0.8988.

Cho et al. (2023) have utilized deep neural networks to analyze the correlation between melt-blown nonwoven fabric production conditions and performance by classifying SEM images. CNN models, including VGG16, VGG19, ResNet50 and DenseNet121, achieved classification accuracies between 0.95 and 0.99. Layer-wise Relevance Propagation (LRP) and Grad-CAM were applied to visualize and interpret SEM image features, enhancing the prediction of production processes. Gotz et al. (2021) introduced the General Image Fiber Tool (GIFT), an advanced method for computerized fiber diameter quantification in SEM images, providing greater accuracy than manual methods and existing tools like DiameterJ. GIFT determines the average fiber diameter and standard deviation through statistical analysis. Comparative tests have shown that GIFT outperformed DiameterJ and manual quantification, especially in challenging image types. Queiroz et al. (2025) explored natural fiber hybrid composites using intralaminar (2D) and orthogonal-through-the-thickness (3D-OTT) reinforcement techniques. Jute fabric was reinforced with sisal, curauá and glass fibers. The composites demonstrated potential to replace glass fiber-reinforced materials (GFRP), with curauá providing similar stiffness and 3D-reinforced sisal offering excellent energy absorption.

Zhang et al. (2025) investigated damage mechanisms during CF/PEEK drilling, focusing on material smearing, burr formation and delamination. It compared twist drills with chip-split grooves and two-step drills. Results show that chip-split grooves reduce temperature and prevent clogging. Twist drills, de-spite applying 0.62 more force, reduce temperature by 0.18%, burr and tear areas by 0.57% and delamination by 0.69. Step drills showed 19% smaller exit delamination but five times larger entrance delamination. Murphy et al. (2020) developed SIMPoly, a Matlab-based tool for measuring fiber diameter in electrospun polymer scaffolds using SEM images. Validated with synthetic images, SIMPoly delivered accurate and consistent measurements with minimal variability between researchers, surpassing the performance of DiameterJ and manual ImageJ methods. It provides a simple and reliable approach for measuring polymer fiber diameter. Padhan et al. (2024) have developed a composite of PBO fibers and PEEK matrix, created in unidirectional (UD) and bidirectional (BD) orientations. The UD composite demonstrated a 10,000% increase in impact strength and a 0.662 increase in tensile strength compared to neat PEEK. Performance was evaluated through hardness, tensile, impact strength and lap shear tests. SEM and micro-CT analysis were employed to study the failure mechanisms.

SEM image segmentation for thermoplastic composites faces challenges such as shine-through artifacts, irregular pores and overlapping fibers. Methods focus on classification, missing detailed segmentation, while struggling with heterogeneous particles. Some of research highlights the lack of damage segmentation. Advanced methods are needed to address these gaps, especially for complex and 3D structures.

3. Materials and Methods

3.1. Material Type and Sample Preparation

SEM sample images belong to material specimens prepared with different production parameters. These images were captured to analyze structural details such as fiber-matrix bonding, micro-cracks, pore formation and fiber fracture mechanisms. In the preparation process of the SEM samples, specimens produced with various parameters were first subjected to tensile and compression tests and then samples were taken from the fracture surfaces. Before SEM analysis, the samples were cut to appropriate sizes, coated with a thin layer of gold or carbon to enhance electron conductivity and imaged under high vacuum conditions. Images captured at different magnification levels provided detailed observations of fiber-matrix interfaces, pores and micro-cracks. In this study images were captured at Ankara University YEBİM using a secondary electron detector to reveal detailed surface morphology. At 2 mm and 200 µm magnification levels, wrinkles were observed in the fiber arrangement, but they had no negative impact on mechanical performance. At 200× magnification, fiber-matrix debonding and localized voids were detected in some areas, although overall bonding appeared strong. Microcracks and matrix separations influenced energy dissipation, leading to controlled fracture behavior. The brittle fracture of fiber ends indicated sudden failure during tensile testing. Additionally, fiber pull-out was observed in certain regions, suggesting localized weak points in load transfer. The scanning mode was set to depth-based and the electron energy was maintained at a high level. The working distance was relatively large, providing a broad field of view. The magnification level was moderate, making it suitable for observing detailed structures. The beam current was kept constant, while the spot size was adjusted to an optimal level. A scale bar was included as a reference to compare structures within the image and facilitate dimensional analysis. The SEM samples used in this study have an original resolution of 1024×946 pixels, providing high-detail microscopic imagery for analysis and segmentation (Figure 1).

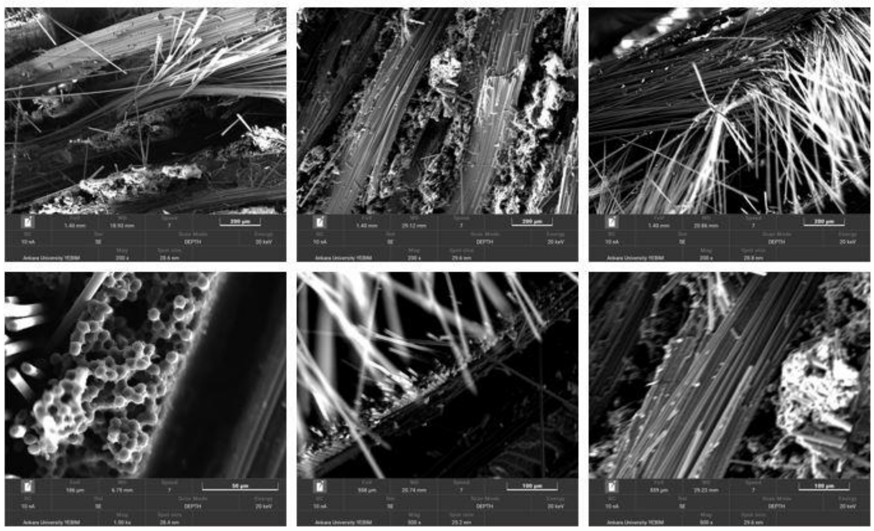

Figure 1. SEM Samples of 1024×946 pixels

3.2. Dataset Creation

Data augmentation techniques have been applied to SEM images, which are known for their high resolution and are commonly used to examine microscopic structures (Shorten., 2019). These techniques help train the model on various images, improving its generalization capability. In this study operations such as rotation, shifting and zooming have been applied to model data from different angles and scales without disturbing the microscopic structure of SEM images. Brightness adjustment and horizontal flipping have also been used to help the model learn how the image appears under varying lighting conditions. Noise addition and blurring techniques have been incorporated to simulate invisible textures. These methods have enhanced the sharpness of fine structures in SEM images, enabling the model to yield accurate results even with diverse and challenging datasets. By applying these data augmentation techniques to SEM images, the model's ability to recognize various microscopic structures has been improved. Additionally, by increasing the diversity of the data, they have helped the model effectively classify low-resolution or noisy SEM images, mitigating overfitting. Ultimately, these techniques have led to more robust and reliable model outputs, better suited for real-world conditions.

The original images are of size 1024×946 pixels and there were 24 original images. These images were divided into 512×512-pixel patches, resulting in 96 images. Following data augmentation, the dataset increased to 186 images, which were used in the final dataset. Each image has been first divided into 512×512 patches and then the dataset has been split into training and validation sets. 80% of the data has been used for training, while 20% has been reserved for validation.

Using a validation set is crucial for ensuring the robustness and generalization of a model. The validation set is used to evaluate the model during training, which helps in tuning hyperparameters, such as learning rate, batch size and model architecture. It provides an unbiased measure of the model's performance on data it hasn't seen before, allowing for an assessment of how well the model is likely to perform on real-world, unseen data. Additionally, the validation set helps in implementing early stopping, which prevents overfitting by halting training when performance on the validation set starts to deteriorate, even if training accuracy continues to improve. This process ensures that the model isn't just memorizing the training data but is learning to generalize to new data. Without a validation set, there is a risk of overfitting, which can lead to poor performance when the model encounters real-world or unseen data.

After splitting, various augmentation techniques have been applied to the images in the training set to enhance the model's ability to generalize across different conditions. The images have been randomly rotated between 0 to 30 degrees, helping the model make accurate predictions from different angles. The images have also been shifted horizontally and vertically by up to 20%, allowing the model to recognize objects in varying positions. Additionally, a zoom effect of up to 20% has been applied, which improves the model's ability to detect objects at different scales. Horizontal flipping has been performed, enabling the model to learn the appearance of objects from both orientations. Lastly, the brightness of the images has been randomly adjusted between 80% and 120%, simulating different lighting conditions and helping the model adapt to varying brightness levels. The validation set has remained unaugmented to ensure an accurate evaluation of the model's performance on real-world, unaltered data. 512×512 pixel patches were extracted from SEM images (Figure 2).

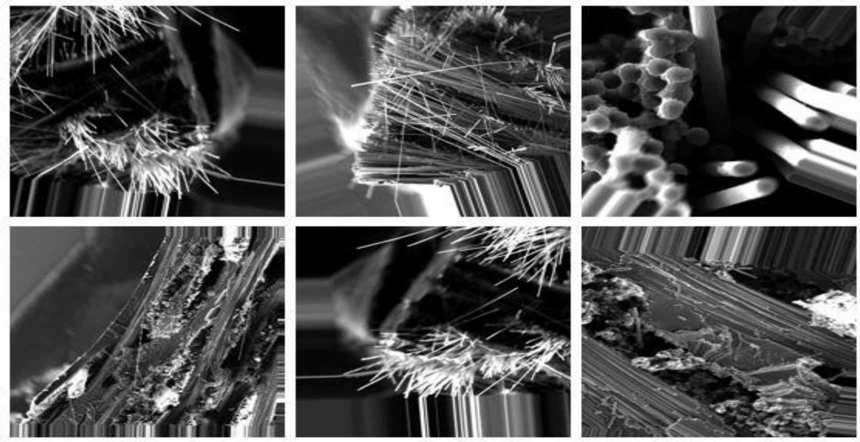

Figure 2. Samples of 512×512 pixels patches

3.3. Model Architecture

3.3.1. U-Net Architecture

U-Net's architecture is distinctive due to its dual-path design, consisting of an encoder and decoder (Figure 3). The encoder extracts contextual information by progressively reducing the spatial resolution of the input while increasing feature depth through convolutional layers. This allows the network to capture abstract representations similar to feedforward layers in conventional convolutional neural networks. Conversely, the decoder reconstructs the segmentation map by upsampling feature maps and refining spatial details. Skip connections link corresponding encoder and decoder layers, ensuring that spatial information lost during encoding is recovered, ultimately improving segmentation accuracy (Ronneberger *et al*., 2015).

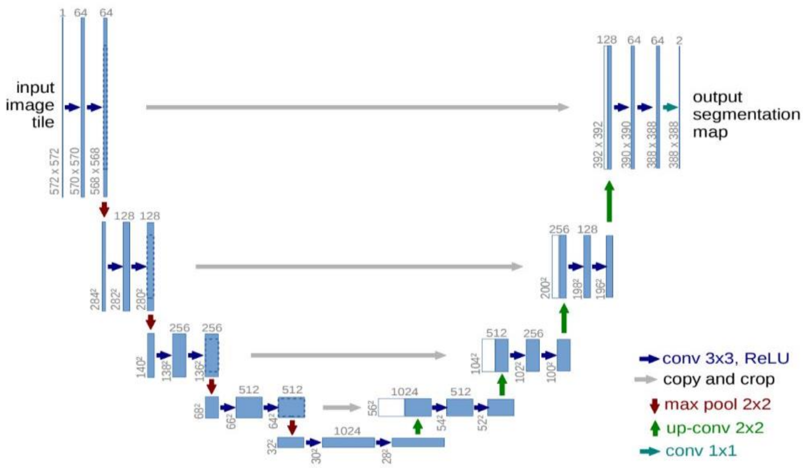

Figure 3. The U-net architecture is shown, with blue boxes representing multi-channel feature maps (channels and dimensions labeled), white boxes for copied feature maps and arrows indicating operations and flow through the network

Figure 3 demonstrates how the U-Net model transforms a grayscale input image of size 572×572×1 into a binary segmented output of size 388×388×2. The reduction in output size occurs due to the absence of padding, which can be adjusted to retain the original dimensions. In the encoder, the input undergoes progressive downsampling, decreasing spatial dimensions while increasing channel depth, enabling the network to extract high-level features. At the bottleneck, a final convolution produces a 30×30×1024 feature map. The decoder then reconstructs the image size through upsampling layers, restoring spatial resolution while reducing channel depth. Skip connections link corresponding layers in both encoder and decoder, preserving spatial details and refining segmentation accuracy. The final output is a binary segmentation map, where each pixel is classified as either foreground or background.

3.3.2. Improved U-Net Model for Segmentation of SEM images of Thermoplastic Composite Rods

In this study, modifications were made to the standard U-Net architecture to enhance its performance, particularly for segmenting SEM images. These modifications were introduced to improve feature extraction, prevent overfitting, preserve spatial information and increase the model's learning capacity.

In this study, a U-Net deep learning model is developed for the segmentation of SEM images. The proposed method consists of three main stages: preprocessing, classical segmentation and deep learning-based segmentation. The improved U-Net model follows 3 stage process for segmenting SEM images of thermoplastic composite rods, enhancing feature extraction and boundary precision (Figure 4).

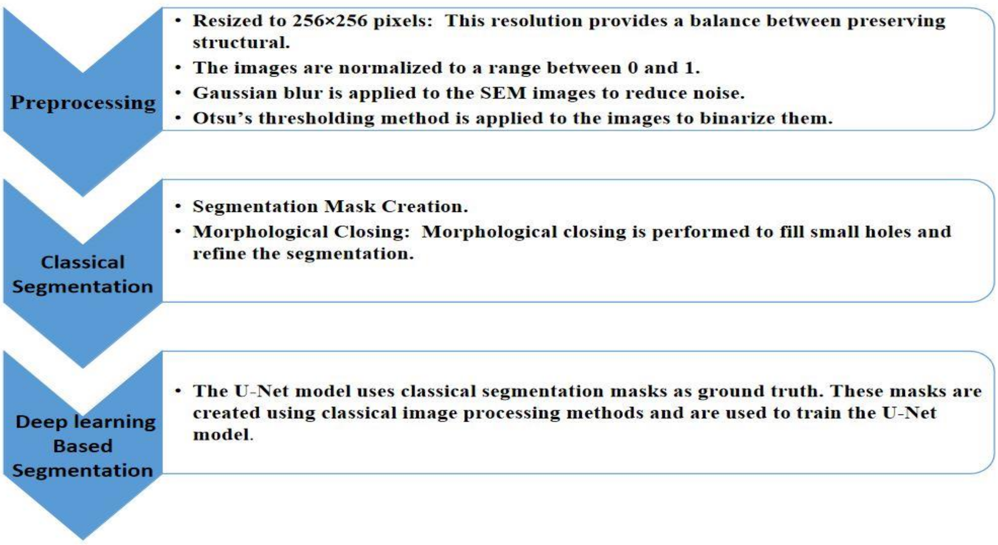

Figure 4. Stages of improved U-Net model for segmentation of SEM images of thermoplastic composite rods

In first stage preprocessing all SEM images undergo an initial preprocessing phase before segmentation. First, all images are resized to 256×256 pixels, ensuring a balance between preserving important structural details, such as particle boundaries and textures, while maintaining efficient training times. Reducing the image size decreases computational cost and enables faster processing during model training. Next, the images are normalized to a range between 0 and 1, ensuring consistent pixel intensity scaling, which helps the model learn effectively. To reduce noise, Gaussian blur is applied, smoothing the images and improving the accuracy of the segmentation process. Finally, Otsu's thresholding is used for binarization, automatically computing an optimal threshold to distinguish the foreground (objects of interest) from the background.

In second stage, Classical segmentation methods are applied to the SEM images to define the segmentation areas quickly. These methods provide initial segmentation masks, which are then used as ground truth labels for the U-Net model during training. Classical image processing methods have been used to generate the segmentation masks. These methods quickly define the regions of interest (Voids of SEM). The classical segmentation masks are compared to the deep learning-based predictions made by the U-Net model. After generating the initial segmentation masks using classical methods, morphological closing is performed to fill small holes and refine the segmentation. This operation helps improve the quality of the mask and ensures better boundary detection. Qualitative comparisons are made by displaying the original SEM images alongside the classical segmentation masks and U-Net predictions. This visual inspection helps in understanding how well the U-Net model performs compared to the classical methods.

In last stage, deep learning-based segmentation is performed using a U-Net architecture designed for semantic segmentation tasks. To enhance segmentation performance, an improved U-Net architecture is implemented with a deeper encoder-decoder structure, incorporating a four-layer encoder with additional convolutional and pooling layers. This deeper design allows the model to extract more complex and hierarchical features from SEM images, capturing fine-grained textures and intricate details. The increased number of layers helps the network learn multi-scale features, improving segmentation performance on high-resolution microscopic images. The encoder consists of convolutional layers with ReLU activation and max-pooling operations for feature extraction, while the decoder utilizes upsampling layers and skip connections to recover spatial information.

To prevent overfitting, dropout layers are added after each convolutional block, randomly deactivating neurons during training and improving generalization, especially when working with limited datasets. This approach is particularly important for SEM images, where high variability in cell structures and textures increases the risk of overfitting. Skip connections with concatenate layers are applied between the encoder and decoder paths, preserving spatial information and preventing the loss of crucial low-level features such as edges and textures during downsampling. These connections ensure precise boundary detection and enhanced segmentation quality. The final segmentation mask is obtained using a 1×1 convolution with a sigmoid activation function, enabling pixel-wise binary classification. The sigmoid function outputs values between 0 and 1, allowing the model to generate clear and accurate binary masks for segmenting objects from the background. The use of sigmoid activation is suitable for medical and scientific imaging tasks, where accurate pixel-level classification is crucial. The model is trained using binary cross-entropy loss and the Adam opti mizer. The improved U-Net architecture incorporates a deeper encoder-decoder structure, additional convolutional and pooling layers, dropout regularization and skip connections to enhance segmentation performance and preserve spatial details (Figure 5).

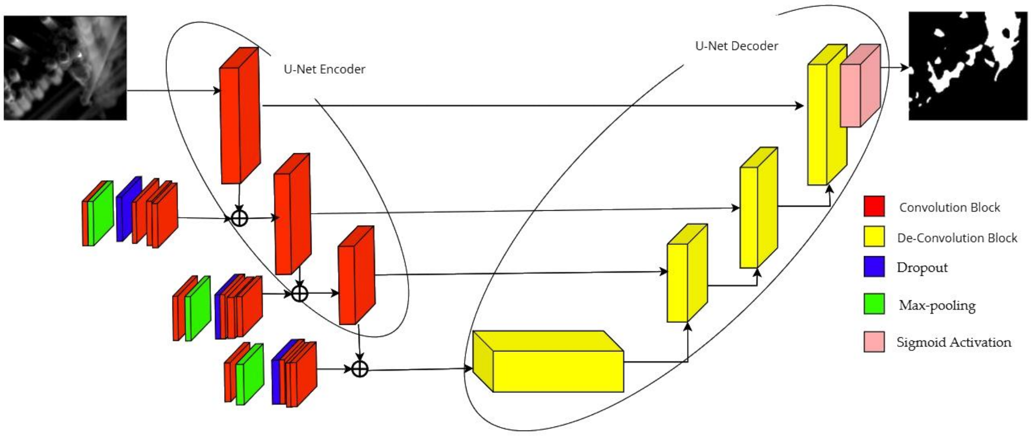

Figure 5. Improved U-Net architecture

Figure 5 shows a U-Net model for segmentation, leveraging its encoder-decoder structure with skip connections for spatial feature preservation. The encoder consists of multiple convolutional blocks (red) that extract hierarchical features, followed by max-pooling layers (green) for spatial down-sampling. To prevent overfitting, dropout layers (blue) are applied during training. In the decoder, deconvolution blocks (yellow) are used to upsample the feature maps, while skip connections concatenate the corresponding encoder features for detailed reconstruction. Finally, a sigmoid activation layer (pink) produces a binary segmentation mask, highlighting the detected regions with pixel-wise probabilities (Equation 1).

$$\sigma(x) = \frac{1}{(1+exp(-x))}\,. \tag{1}$$

It maps any input x to a value between 0 and 1, making it suitable for binary segmentation tasks by assigning pixel-wise probabilities.

3.4. Performance Evaluation Metrics

The F1-Score, a weighted average of precision and recall, is a widely used evaluation metric in current research on segmentation of SEM images. Consequently, this study employs the following definitions for precision, recall and F1-Score.

$$Recall = \frac{TP}{TP+FN}\,, \tag{2}$$

$$Precition = \frac{TP}{TP+FP}\,, \tag{3}$$

$$F1 - Score = 2 \times \frac{precision \times recall}{precision + recall}\,. \tag{4}$$

Accuracy is a performance metric that measures how well a model correctly classifies instances. It is defined as the ratio of correctly predicted outcomes, including both True Positives (correctly identified positive cases) and True Negatives (correctly identified negative cases), to the total number of instances. The formula for accuracy is:

$$Accuracy = \frac{TP+TN}{TP+TN+FP+FN}. \quad (5)$$

The Jaccard Index measures the overlap between predicted and ground truth regions in image segmentation. It is calculated by dividing the intersection (A∩B) of the predicted and actual pixels by their union (A ∪ B). The Jaccard Index ranges from 0 (no overlap) to 1 (perfect overlap) and is widely used to evaluate segmentation accuracy in computer vision tasks.

$$Jaccard\ Index = \frac{A \cap B}{A \cup B}. \quad (6)$$

4. Result and Discussion

4.1. Experiment Results

We conduct the experiments on the Colab platform with a PC, including an NVIDIA RTX 4000 GPU, Intel(R) Xeon(R) W-2245 CPU@3.90GHz and 64GB System RAM. The improved U-Net model was configured with the Adam optimizer using a learning rate of 0.001. The training was conducted over 4 epochs with a batch size of 2. Table 1 shows results of data accuracy for improved U-Net by varying epochs.

Table 1. Results of SEM data for varying epochs

	Metrics		
Epoch	**F1-Score**	**Accuracy**	**Jaccard Index**
10	0.8397	0.8930	0.7237
30	0.8373	0.8853	0.7201
50	0.8518	0.9024	0.7418
100	**0.8537**	**0.9371**	**0.7448**

Table 1 presents the performance metrics of the SEM model across different training epochs, including F1-Score, accuracy and Jaccard Index. The performance metrics of the model across different epochs indicate steady improvement, particularly in accuracy and Jaccard index, while the F1-score shows slight fluctuations.

The F1-Score starts at 0.8397 in epoch 10, peaks at 0.8537 by epoch 100, showing an overall improvement. This slight increase suggests that the model is gradually improving its ability to balance precision and recall in segmentation tasks. However, the small variation between epoch 10 and 30 (0.8397 to 0.8373) indicates that the model may have experienced a slight dip in its precision-recall trade-off early on but quickly recovered and continued to improve with further training. The accuracy metric shows consistent growth, increasing from 0.8930 at epoch 10 to 0.9371 at epoch 100. This significant improvement reflects the model's ability to correctly classify more pixels in the segmentation process over time. The continuous rise in accuracy is a positive indication that the model is learning better general features of the SEM images and refining its predictions. The Jaccard Index, a measure of overlap between predicted and ground truth segmentation masks, also shows improvement from 0.7237 at epoch 10 to 0.7448 at epoch 100. The slight but steady increase in Jaccard Index suggests that the model is improving its ability to accurately segment the objects of interest, maintaining a good balance between detecting true positives and minimizing false positives.

Overall, the results demonstrate that the model is learning effectively across training epochs. The improvements in both accuracy and the Jaccard index imply better segmentation performance over time. The relatively small variations in F1-score between epochs 10 and 30, followed by a steady rise afterward, suggest that the model had to adjust and refine its learning strategy to optimize for both precision and recall. Figure 6 illustrates the segmentation voids in SEM images, with some sections highlighted using red arrows. (a) shows the original SEM images, (b) displays the classic mask segmentation and (c) presents the improved U-Net segmentation.

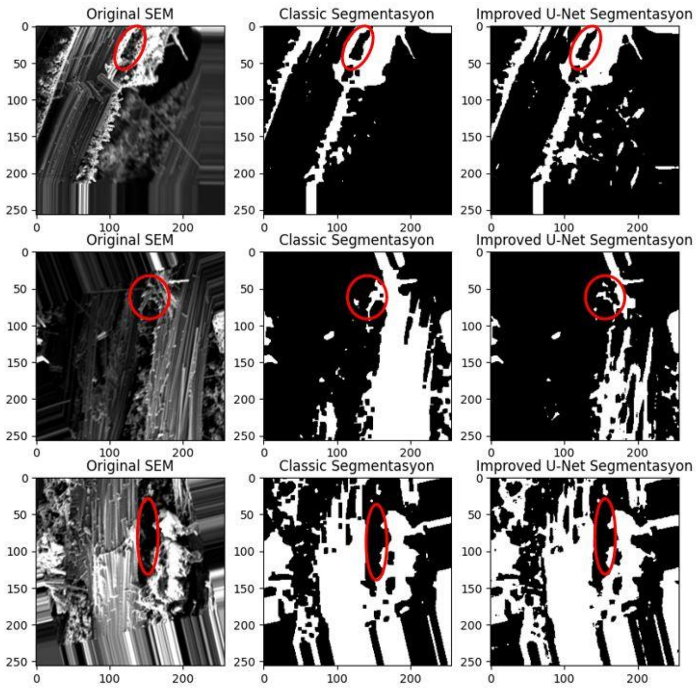

Figure 6. Samples segmentation voids of SEM images that some of section shows with red circles (a) Original SEM images; (b) Classic mask segmentation; (c) Improved U-Net segmentation

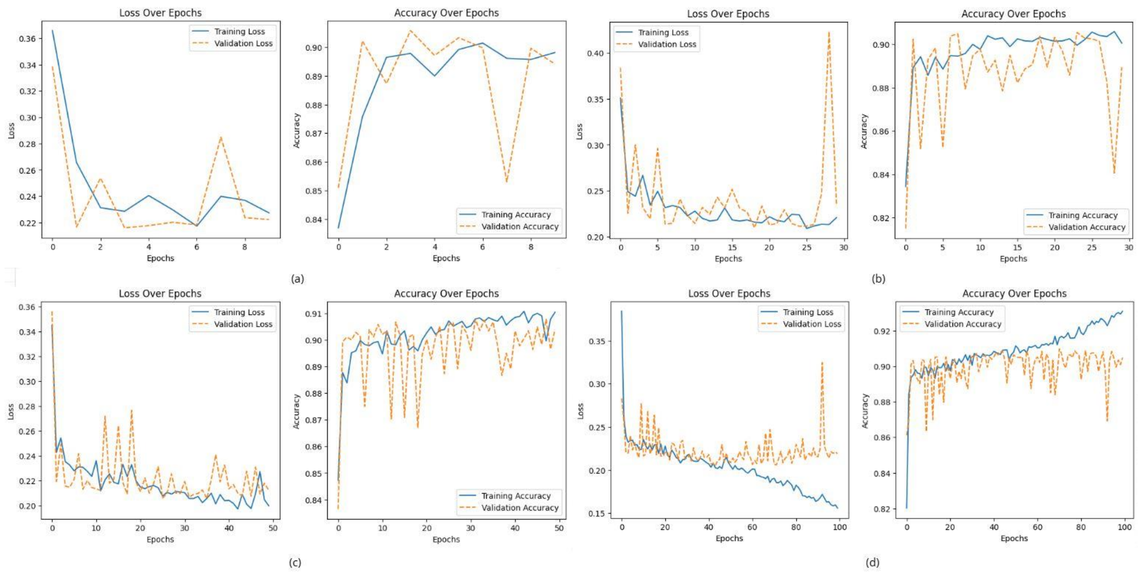

Figure 7. Training and validation loss: (a) 10 epoch; (b) 30 epoch; (c) 50 epoch and (d) 100 epoch

Figure 7 presents the training and validation loss at different epochs: (a) 10 epochs, (b) 30 epochs, (c) 50 epochs and (d) 100 epochs. The images used in the model were resized to 256×256 pixels and the model's accuracy was evaluated using epoch sizes of 10, 30, 50 and 100. Epoch (a) suggests potential overfitting, with the training loss decreasing and training accuracy increasing sharply. However, the validation loss starts to rise after a few epochs and validation accuracy plateaus or slightly declines. This divergence between training and validation metrics indicates the model is memorizing the training data rather than generalizing. Potential solutions include regularization, dropout, early stopping, data augmentation and model simplification. Epoch (b) demonstrates better generalization, with both training and validation losses decreasing. The validation loss fluctuates initially, but both training and validation accuracies increase, with the validation accuracy closely tracking the training accuracy. This suggests good learning but potential slight overfitting or incomplete learning. To improve, further investigation into the initial validation loss spike, hyperparameter tuning and careful monitoring are recommended. In epoch (c), the training loss decreases while the validation loss, after an initial dip, begins to fluctuate and slightly rise, suggesting overfitting. The training accuracy nears 100%, but the validation accuracy plateaus at a lower level. Epoch (d) exhibits better generalization, with both training and validation losses decreasing and converging. Although minor spikes occur in the validation loss, both training and validation accuracies increase steadily and the validation accuracy reaches a high level. The gap between training and validation metrics is smaller than in (c), indicating better generalization. For epoch (c), potential solutions for overfitting include regularization, dropout, early stopping, data augmentation and model simplification.

4.2. Visualization Analysis

The visualization of SEM images was achieved using an improved U-Net model applied to the Grad-CAM framework. This choice was made due to several advantages, including its straightforward implementation, well-structured yet flexible architecture and high interpretability. These attributes make U-Net ideal for generating explainable visualizations, as it effectively highlights the regions that contribute the most to the model's decision-making process. The colored areas indicate the significance of specific regions in influencing the model’s predictions, with warmer colors (red and yellow) representing regions with higher influence and cooler colors (blue and green) indicating areas of lower relevance. This approach enhances the interpretability of the deep learning model by providing insights into how the network processes SEM images and identifies critical features. By leveraging Grad-CAM heatmaps, researchers can better understand the decision-making patterns of the model, ensuring transparency and aiding in the refinement of the system for improved accuracy and reliability. The heatmap emphasizes key structural features, such as the fiber-matrix interfaces, which are critical for assessing the bonding quality and mechanical performance of the composite. Additionally, areas of potential voids or defects are highlighted, which can impact the material’s strength and durability. The model's attention to these specific regions offers valuable insights into the composite's microstructural integrity and guides further optimization of processing conditions or material design. This heatmap helps in visualizing how well the model has learned to detect important microstructural characteristics that influence the overall performance of thermoplastic composites under various stress and loading conditions. Figure 8 presents the Grad-CAM visualizations obtained from the improved U-Net model, with overlaid heatmaps illustrating the activation intensities across different regions of the SEM images.

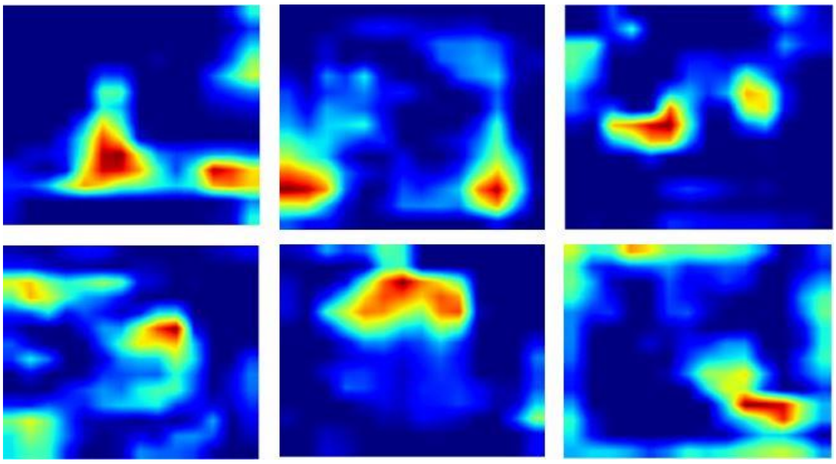

Figure 8. Grad-CAM Heatmap for SEM images

4.3. Comparison of the Obtained Results

Table 2 presents a comparative evaluation of different segmentation methods, including Optical Flow-based, U-Net, PSPNet, U-Net-based and the proposed improved U-Net model. The comparison is based on three key performance metrics: Accuracy, Jaccard Index and F1-Score. The Optical Flow-based method achieved an accuracy of 0.866, demonstrating its effectiveness in segmentation but lacking reported Jaccard and F1-Score values for further assessment. The standard U-Net, a widely used deep learning model, obtained an accuracy of 0.762 and a Jaccard Index of 0.806, indicating good region overlap performance. However, its accuracy was lower compared to the Optical Flow-based method. PSPNet performed moderately, with a Jaccard Index of 0.6243 and an F1-Score of 0.6362, suggesting a lower segmentation quality. Similarly, the U-Net-based method recorded a Jaccard Index of 0.53 and an F1-Score of 0.67, showing weaker performance. The proposed improved U-Net significantly outperformed the other methods, achieving the highest accuracy of 0.9371, indicating superior classification performance. It also demonstrated strong segmentation quality with a Jaccard Index of 0.7448, which, while slightly lower than U-Net's 0.806, still reflects a well-balanced trade-off between boundary precision and segmentation consistency. Furthermore, the Proposed U-Net obtained the highest F1-Score of 0.8537, confirming its ability to maintain an effective balance between precision and recall. These results highlight the robustness and reliability of the proposed improved U-Net model in segmentation tasks, making it the most effective method among those compared. Although there is a minor trade-off in Jaccard Index compared to the standard U-Net, the overall improvements in accuracy and F1-Score indicate its superiority in achieving precise and consistent segmentation.

Table 2. Comparison the obtained results with the literature

Methods	Accuracy	Jaccard Index	F1-Score
Optical flow-based (Moroni & Thiele, 2020)	0.866	-	-
Standard U-Net (Badran *et al*., 2022)	0.762	0.806	-
PSPnet (Zhang *et al*., 2025)	-	0. 6243	0.6362
U-Net based (Beskopylny *et al*., 2023)	-	0.53	0.67
Improved U-Net	**0.9371**	**0.7448**	**0.8537**

5. Conclusions

In this study, a deep learning-based SEM image analysis has been conducted to evaluate the microstructural properties of the thermoplastic composite rod surfaces in samples subjected to tensile testing. To this end, this study has proposed, U-Net deep learning model for the segmentation of SEM images of thermoplastic composite rod surfaces. The proposed model has integrated the attention mechanisms and residual blocks to improve feature refinement and segmentation accuracy in complex microstructural regions. The results demonstrate that the improved U-Net achieves high accuracy and robustness in segmenting the thermoplastic composite rods, outperforming conventional image processing techniques. Additionally, the application of Grad-CAM for explainability has provided the insights into the model's decision-making process. The findings suggest that the proposed approach can be effectively used for automated analysis of composite microstructures, aiding in material characterization and defect detection. Future research could explore further enhancements through hybrid architectures and self-supervised learning techniques to improve generalization across diverse datasets.

References

Badran, A., Parkinson, D., Ushizima, D., Marshall, D. & Maillet, E. (2022). Validation of deep learning segmentation of CT images of fiber-reinforced composites. *Journal of Composites Science*, *6*(2), 60.

Beskopylny, A.N., Shcherban', E.M., Stel'makh, S.A., Mailyan, L.R., Meskhi, B., Razveeva, I., ... & Artamonov, S. (2023). Method for concrete structure analysis by microscopy of hardened cement paste and crack segmentation using a convolutional neural network. *Journal of Composites Science, 7*(8), 327.

Butenegro, J.A., Bahrami, M., Swolfs, Y., Ivens, J., Martínez, M.Á. & Abenojar, J. (2023). Novel sustainable composites incorporating a biobased thermoplastic matrix and recycled aerospace prepreg waste: Development and characterization. *Polymers*, *15*(16), 3447.

Cho, K.C., Park, S.W., Lee, I. & Shim, J. (2023). Process prediction and feature visualization of meltblown nonwoven fabrics using scanning electron microscopic (SEM) image-based deep neural network algorithms. *Processes*, *11*(12), 3388.

De Queiroz, H.F.M., dos Santos, N.V., Neto, J.S.S. & Banea, M.D. (2025). Mechanical characterization of novel natural fibre-reinforced composites via a three-dimensional fibre architecture. *Composites Science and Technology*, 261, 110996.

Diniță, A., Ripeanu, R.G., Ilincă, C.N., Cursaru, D., Matei, D., Naim, R.I., ... & Portoacă, A.I. (2023). Advancements in fiber-reinforced polymer composites: A comprehensive analysis. *Polymers*, *16*(1), 2.

Dubey, D., Singh, S.P. & Behera, B.K. (2025). Mechanical, thermal and microstructural analysis of 3D printed short carbon fiber-reinforced nylon composites across diverse infill patterns. *Progress in Additive Manufacturing*, *10*(2), 1671-1689.

Elderfield, N., Cook, O. & Wong, J. C. (2024). Fiber dispersion as a quality assessment metric for pultruded thermoplastic composites. *Composites Part B: Engineering*, 275, 111321.

Götz, A., Senz, V., Schmidt, W., Huling, J., Grabow, N. & Illner, S. (2021). General image fiber tool: A concept for automated evaluation of fiber diameters in SEM images. *Measurement*, 177, 109265.

Jin, Z., Han, Z., Chang, C., Sun, S. & Fu, H. (2022). Review of methods for enhancing interlaminar mechanical properties of fiber-reinforced thermoplastic composites: Interfacial modification, nano-filling and forming technology. *Composites Science and Technology*, 228, 109660.

Lu, S., Zhao, X., Liu, H. & Liang, H. (2024). Semiconductor material porosity segmentation in flame retardant materials sem images using data augmentation and transfer learning. In *Computer Systems and Communication Technology*, 74-81. IOS Press.

Mohsenzadeh, R., Soudmand, B.H., Najafi, A. & Hazzazi, F. (2024). Morphology-driven nanofiller size measurement integrated with micromechanical finite element analysis for quantifying interphase in polymer nanocomposites. *ACS Applied Materials & Interfaces*, *16*(30), 39927-39941.

Moroni, R., Thiele, S. (2020). FIB/SEM tomography segmentation by optical flow estimation. *Ultramicroscopy*, 219, 113090.

Padhan, M., Marathe, U. & Bijwe, J. (2024). Developing superperforming composites by harnessing fiber orientation and processing technology. *ACS Omega*, *9*(32), 34281-34291.

Ronneberger, O., Fischer, P. & Brox, T. (2015). U-net: Convolutional networks for biomedical image segmentation. In *Medical Image Computing and Computer-Assisted Intervention–MICCAI 2015: 18th International Conference Proceedings*, 234-241. Springer International Publishing.

Samet, K., Kocak, H. & Karatas, C. (2024). Thermoplastic composite push-pull rod manufacturing technologies and current applications. *Current Reviews in Materials Science Engineering*, 167-228. (In Turkish).

Shorten, C., Khoshgoftaar, T.M. (2019). A survey on image data augmentation for deep learning. *Journal of Big Data*, *6*(1), 1-48.

Tucci, F., Rubino, F., Pasquino, G. & Carlone, P. (2023). Thermoplastic pultrusion process of polypropylene/glass tapes. *Polymers*, *15*(10), 2374.

Vaidya, U., Ning, H., Janney, M., Mauhar, M., Graham, K. & Streckel, M. (2023). Thermoplastic composite connecting rods. *Composites Part B: Engineering*, 252, 110518.

Wu, J. (2017). *Introduction to Convolutional Neural Networks*. National Key Lab for Novel Software Technology, Nanjing University, 31.

Zhang, X., Chen, J., Wang, H., Ma, T., Lin, L., Yang, L., ... & Chen, M. (2025). Mechanisms of defect formation and evolution in drilling thermoplastic CF/PEEK composite using twist and step drills. *Composite Structures*, 355, 118833.

Zhang, X., Wei, B., Hao, K., Gao, L., Xie, R. & Wang, H. (2025). Micro-KTNet: Microstructure knowledge transfer learning for fiber masterbatch agglomeration recognition. *Journal of Industrial Textiles*, 55, 15280837241307864.